[2]Van Driest, E. R., "On Turbulent Flow Near a Wall," *Journal of the Aeronautic Science,* Nov. 1956, pp. 1007–1011.

[3]Laufer, J., "The Structure of Turbulence in Fully Developed Pipe Flow," NACA TR-1174, Oct. 1954.

[4]Spalding, D. B., "Heat Transfer from Turbulent Separated Flows," *Journal of Fluid Mechanics,* Vol. 27, Jan. 1967, pp. 97–109.

[5]Launder, B. E., and Spalding, D. B., "The Numerical Computation of Turbulent Flows," *Computer Methods in Applied Mechanics and Engineering,* Vol. 3, March 1974, pp. 269–289.

[6]El-hawary, M. A., and Nicoll, W. B., "A Relation for the Length-Scale of Turbulent to Mean Flow Characteristics Close to the Wall," *Letters in Heat and Mass Transfer,* Pergamon, Vol. 7, Nov. 1980, pp. 401–411.

[7]Chieng, C. C., and Launder, D. B., "On the Calculation of Turbulent Heat Transport Downstream from an Abrupt Pipe Expansion," *Numerical Heat Transfer,* Vol. 3, April 1980, pp. 189–201.

[8]Pope, S. B., and Whitelaw, J. H., "The Calculation of Near-Wake Flows," *Journal of Fluid Mechanics,* Vol. 73, Jan. 1976, pp. 9–32.

[9]Launder, B. E., "Second Momentum Closure: Methodology and Practice," Proceedings of the Ecole d'Et'e d'Analyse Numerique-Modelisation Numerique de la Turbulence, France, 1982.

[10]Patel, V. C., Rodi, W., and Scheuerer, G., "Turbulence Models for Near-Wall and Low Reynolds Number Flows: A Review," *AIAA Journal,* Vol. 23, No. 9, 1985, pp. 1308–1319.

[11]Wilcox, D. C., "Reassessment of the Scale-Determining Equation for Advanced Turbulence Models," *AIAA Journal,* Vol. 26, No. 11, 1988, pp. 1299–1310.

[12]Derksen, R. W., and Azad, R. S., "Behavior of the Turbulent Energy Equation at a Fixed Boundary," *AIAA Journal,* Vol. 19, No. 1, 1981, pp. 238–239.

[13]Schlitchting, H., *Boundary Layer Theory,* McGraw-Hill, New York, 1979.

[14]Mansour, N. N., Kim, J., and Moin, P., *AIAA Journal,* Vol. 27, No. 8, 1989, pp. 1068–1073.

Three-Dimensional Visualization of Temporal Flow Sequences

I. van Cruyningen,* A. Lozano,* M. G. Mungal,† and R. K. Hanson‡
High Temperature Gasdynamics Laboratory
Stanford University, Stanford, California 94305

Introduction

FLOW visualization remains one of the most powerful methods of gaining insight into turbulent flow physics. Recently there have been several excellent reviews[1-3] that describe some of the latest developments in the field. It is also well known among the research community that movie or video sequences of flow visualization images, because of their dynamic nature, are frequently used to study flow development. Presentation of these data as a series of successive frame-by-frame images allows some correlation of temporal information, but is generally unsatisfactory as the human eye is much more adept at determining spatial correlations within a single image. This note describes the application of a method to generate single three-dimensional views that emphasize temporal correlations of time-evolving two-dimensional data sets (i.e. movies), thereby improve interpretation of such data.

Received Dec. 15, 1989; revision received Feb. 19, 1990; accepted for publication March 20, 1990.

*Research Assistant, Department of Mechanical Engineering.

†Assistant Professor, Department of Mechanical Engineering. Member AIAA.

‡Professor, Department of Mechanical Engineering. Member AIAA.

To generate the new views, the separate images are first stacked to form a data volume composed of the downstream spatial (x), cross-stream spatial (y), and time (t) dimensions. High-resolution volume rendering is used to extract constant property surfaces from this three-dimensional data volume. The resulting surfaces are shaded owing to a light source placed to the side of the viewing direction and projected onto the computer display. Temporal correlations, such as the movement of organized (coherent) structures, are then readily perceived. The method is illustrated with three specific examples of round jet flows: a forced low speed jet, a very high Reynolds number rocket motor exhaust jet, and a turbulent jet diffusion flame. It will be seen that, with volume rendering, interpretation of the flow physics is greatly improved, more so than was previously possible.

In related earlier work, Jimenez et al.[4] and Agui and Hesselink[5] stacked sequential cross-stream slices of a mixing layer and a low Reynolds number jet, respectively. Both of these data sets show y-z views of the flow at a fixed downstream station as a function of time t. Polygonal or cylindrical approximations to the surfaces were extracted from the y-z-t data volumes and were displayed with vector graphic techniques. The resulting images provided very useful information about the structures that are advected past the fixed downstream location. By contrast, in the present work, slices through the centerline of the flow are stacked to form x-y-t data volumes so that information for all downstream locations is available in one view. This perspective is found to be more amenable to studies of flow evolution.

Approach

In our work, an improved voxel-based (volume element) rendering algorithm[6] was used to reduce the data volumes on a PIXAR Image Computer with SUN 3/160C host. The algorithm operates on slices through the data volume with the light source direction and observation direction first selected. The slice orientation is then aligned with rays from the observation point to allow rapid final projection. Each slice and its two neighboring slices are mapped through a concentration threshold function, and the three-dimensional gradient of the mapped pixels is determined. The locations of the maximum magnitude of the gradient determine the rendered surface, whose normal is used to calculate the reflection of a collimated beam from the light source direction into the observation direction. Finally, the reflections from all surfaces in a given slice are summed towards the observation direction to produce one scan line for the display. Note that surfaces and normals are calculated at pixel resolutions so the rendered images retain the full resolution of the original data. No geometric approximations to the surface are made, which results in a faithful representation of the rendered surface.

To assist in understanding the fluid motion, depth cues due to shading are further enhanced by calculating numerous perspectives and allowing interactive rotation of the resulting views. The rotating volumes accentuate features observed in the static views presented here and are best observed directly on the computer screen or in video format.[7] Although, as discussed in Ref. 1, there is no effective way to archive video images in technical publications, volume renderings as used here may prove to be the next best substitute.

Results

Figure 1a illustrates a sequence of movie frames of a forced jet. These images were produced through a combination of planar laser-induced fluorescence and phosphorescence of a forced nitrogen jet flow[8] seeded with 5% mole fraction biacetyl (2-3 Butanedione). The jet issued at 85 cm/s (Re = 360) into a nitrogen coflow of 5.4 cm/s and was forced by a loudspeaker at 85 Hz (jet Strouhal number, St = 0.6) to produce the mushroom shaped vortical structures which convect downstream. Shown here are nine frames, each of 384 × 576 pixels, spanning one complete forcing cycle and seven down-

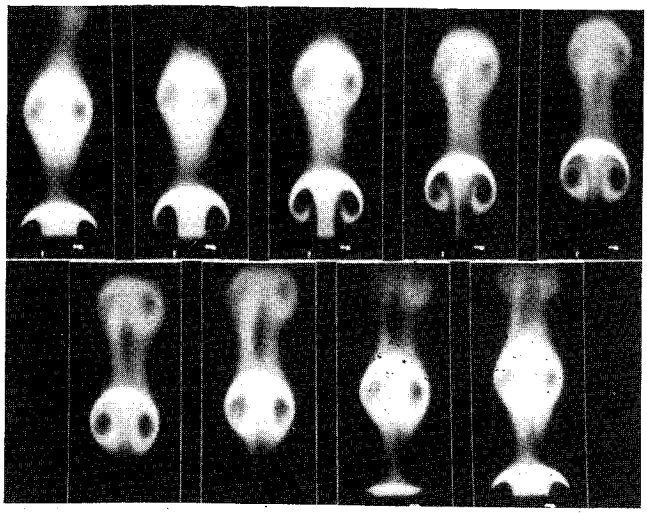

Fig. 1a Movie sequence of nine images of a low-speed forced jet flow (Re = 360, St = 0.6, 7 jet diam field of view, ~1 long time scale displayed).

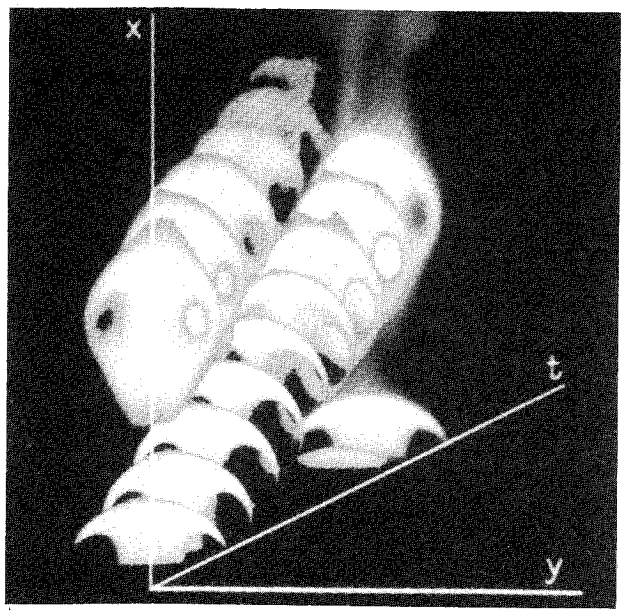

Fig. 1b Stacking procedure.

stream diameters. These images show the conventional movie sequence, with the cycle repeating on the ninth frame.

Figure 1b illustrates the procedure for stacking of the individual x-y image planes to produce a three-dimensional x-y-t volume. The final volume rendering, Fig. 1c, shows the 1% biacetyl iso-concentration surface as a solid body with all hidden surfaces removed. The propagation of and changes to the large vortical structures as defined by the 1% contour is clearly seen. For this simple example, the rendered image, when compared with the movie sequence of Fig. 1a, begins to illustrate the ease of extraction of organized motion and resulting flow physics.

A more challenging example of volume rendering is seen in Fig. 2, which shows two views of the exhaust plume from the test firing of a TITAN IV rocket motor. The resulting momentum driven jet had a Reynolds number of 1.8×10^8, and the field of view shown here extends from 120 to 610 m (140 to 715 jet diam) downstream from the nozzle. The alumina particles in the exhaust absorbed and scattered direct sunlight, which was observed with a video camera.[9] This rendering was produced from 210 images of the resulting movie sequence and covers 21 s of burn. The largest characteristic time scale in the flow can be estimated from the plume width and velocity at

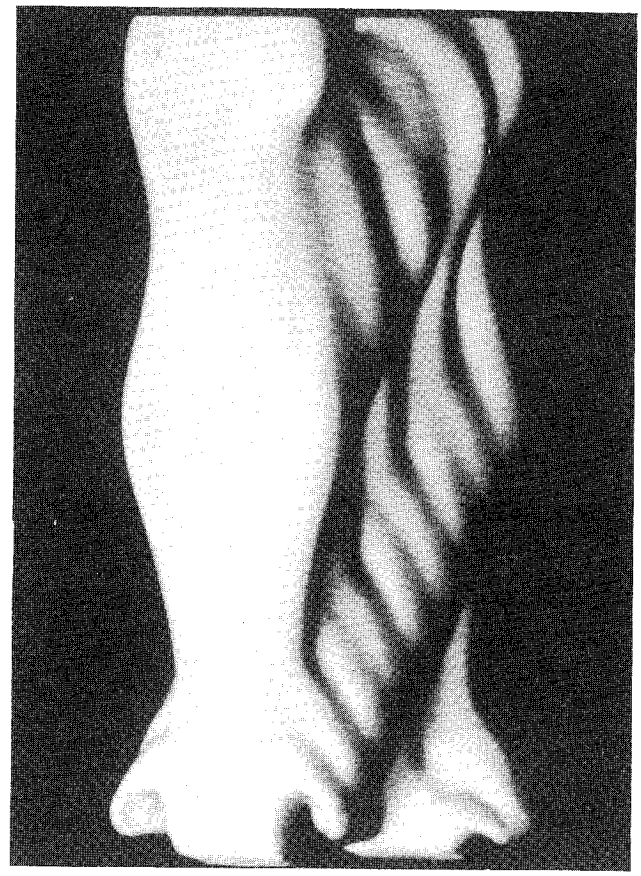

Fig. 1c Volume rendering.

the top of the field of view. The plume width can be measured to be approximately 240 m, and the velocity can be calculated by assuming a constant momentum flux and a Gaussian mean velocity profile. For a velocity estimate of 28 m/s, the local time scale estimate is 9 s, so the rendered image encompasses approximately two and a third of the longest time-scales.

The reader is able to note the significant detail and structure observable in the rendered images, which to our knowledge have not been as clearly demonstrated before. The slope of the diagonal lines, representing organized motions, reduces according to the $1/x$ self-similar decay in velocity, and the length scale of the structures increases linearly with x as required for self-similar growth. Other notable features are the occurrence of occasional pairings whereby two structures coalesce into a single new structure. These features are quite difficult to observe in the original video data.[9] Further discussion of this flow is given in Ref. 10, where it is demonstrated that the features discussed above are not an artifact of the chosen scalar contour. These images also establish, in an unambiguous way, that organized structures exist in momentum driven jet flows at very high Reynolds numbers and are similar to those observed in low Reynolds number flows.[11] Thus, the organized motions seen here in the jet far-field result from inviscid instability mechanisms and are not a remnant of transitional behavior.[9]

The final example of volume rendering is seen in Fig. 3, which shows two views of an ethylene jet diffusion flame[12] at a cold flow Re = 5700. The natural soot emission of this flame was observed with a high speed motion analysis video system (Kodak Spin Physics SP2000) at 200 frames per s. This rendering was produced from 150 consecutive frames of the 192×238 pixel images with a field of view of 260 jet diam. The characteristic time scale at the tip was approximately 0.07 s, so the rendering covers approximately 10 of the largest characteristic times. The organized structures are again very evident as bands that travel up through the flame body. These

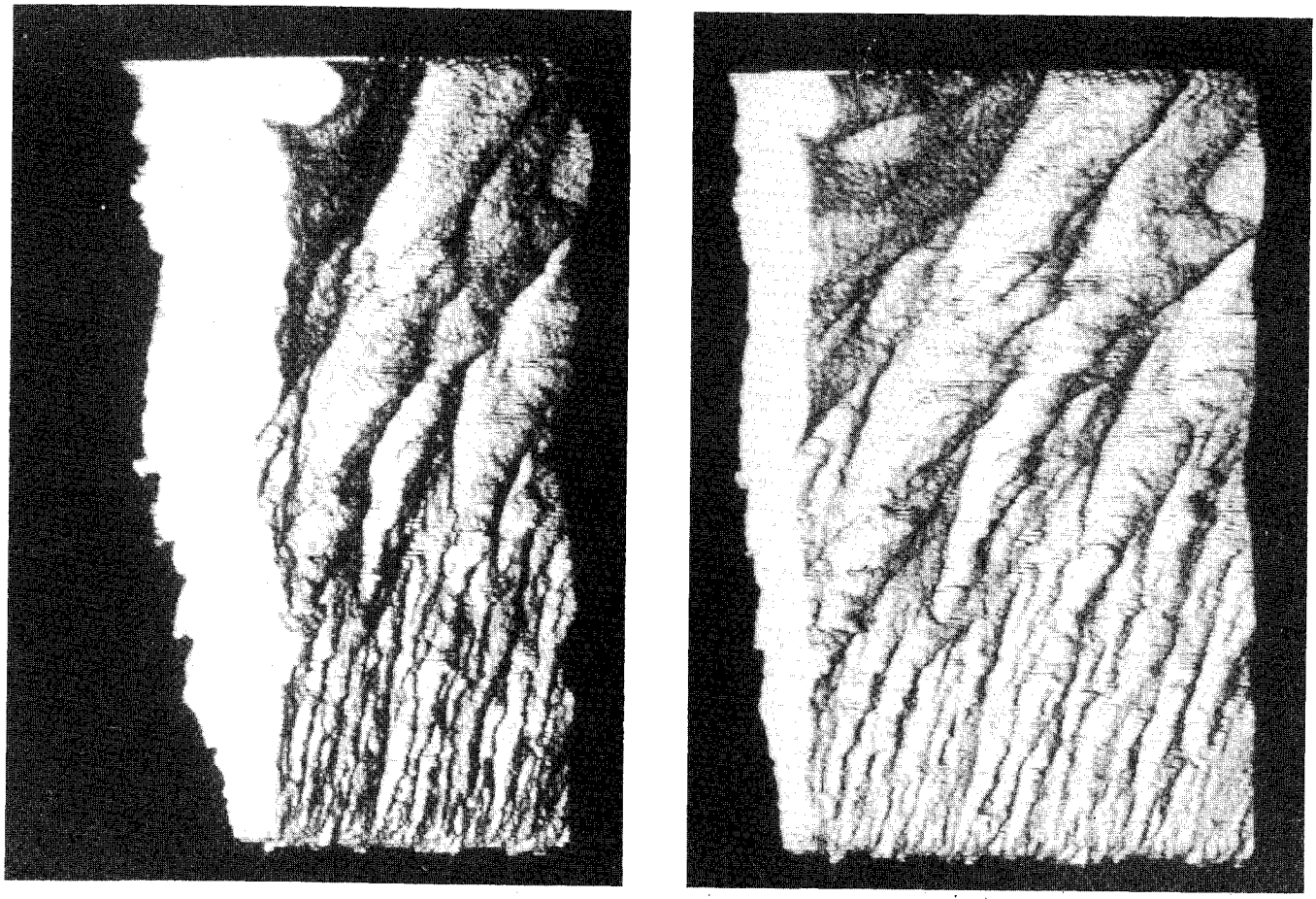

Fig. 2 Volume rendering of 210 images of a rocket motor exhaust jet viewed at 38 and 68 deg off the time axis ($Re = 1.8 \times 10^8$, 140 to 710 jet diam field of view, ~ 2 and 1/3 long time scales displayed).

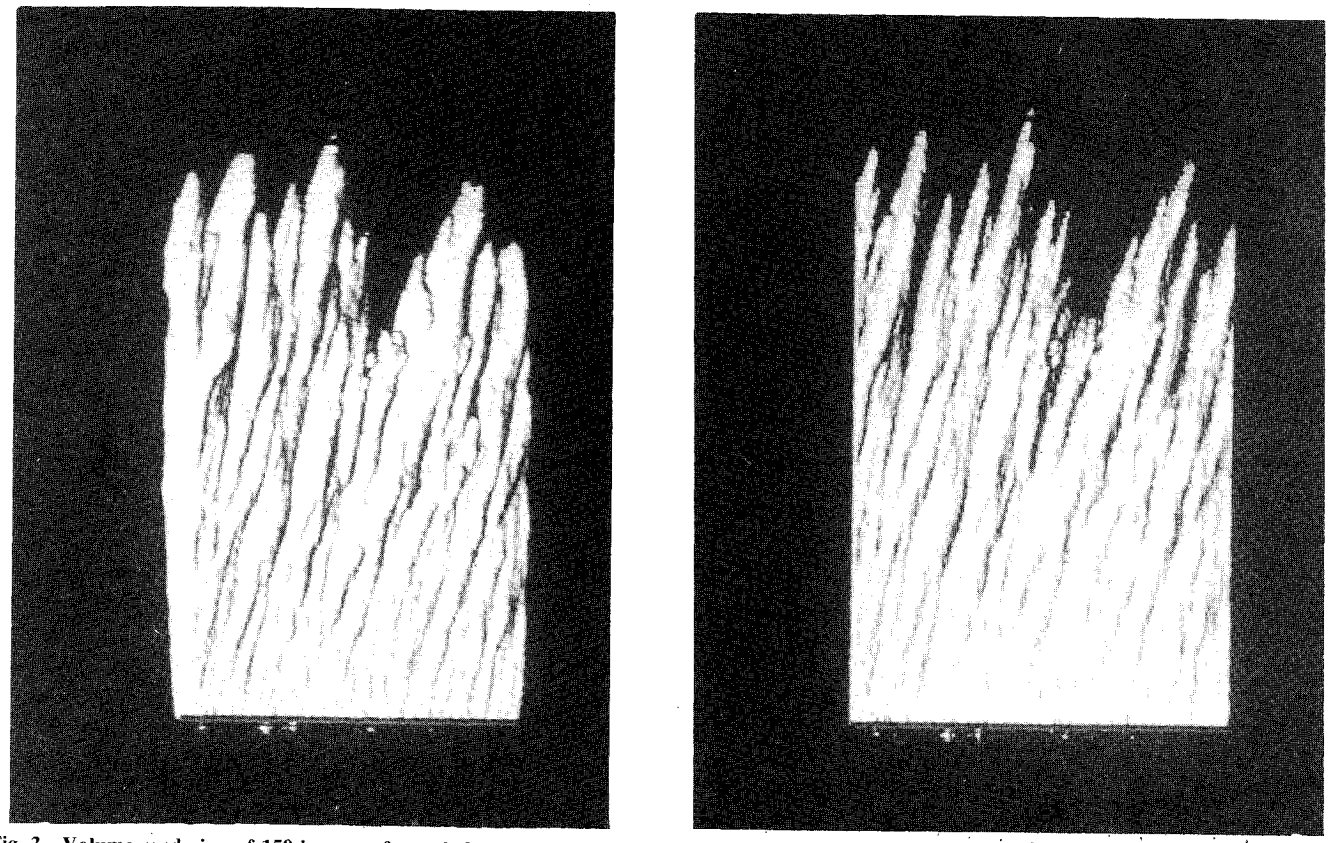

Fig. 3 Volume rendering of 150 images of an ethylene diffusion flame viewed at 70 and 90 deg off the time axis ($Re = 5700$, 260 jet diam field of view, ~ 10 long time scales displayed).

structures eventually become the flame tip which is seen to burn out in a quasiperiodic fashion. Thus, the instantaneous flame length does not vary in a purely random fashion but is a consequence of the organized motion in the flow. These images provide some of the clearest evidence to date to link the underlying organized motion and the resulting flame tip oscillation. Reference 12 also shows that the period of the flame tip oscillation scales properly with the local large-scale variables. Thus, while organization in the near-field is well-established,[13] images such as the ones shown in Fig. 3, begin to demonstrate the combustion implications of the organization that is seen in the jet far-field as illustrated in Fig. 2. Similar findings have been reported in Ref. 14 for liquid jet studies.

Conclusions

The rendering of image sequences used here is of great value in finding temporal correlations in data sequences, as it provides an integrated, global view of the time evolution as opposed to the single instant views produced by a movie loop. By first examining the development of a pulsed low Reynolds number jet, one is able to make the connection between the conventional movie sequence and the new rendered images. Volume renderings of images of a very high Reynolds number jet and a turbulent diffusion flame clearly illustrate organized motions that are more difficult to discern in direct movie projections. The method, we believe, should be equally beneficial when applied to movie sequences of other flows of scientific and technological interest. Although not shown here, the method appears equally applicable to computational results.

Acknowledgment

This research was sponsored by the Air Force Office of Scientific Research, Aerospace Sciences Directorate.

References

[1]Settles, G. S., "Modern Developments in Flow Visualization," *AIAA Journal*, Vol. 24, Aug. 1986, pp. 1313–1323.

[2]Gad-el-Hak, M., "Visualization Techniques for Unsteady Flows: An Overview," *Journal of Fluids Engineering*, Vol. 110, Sept. 1988, pp. 231–243.

[3]Miles, R. B., and Nosenchuck, D.M., "Three Dimensional Quantitative Flow Diagnostics," *Lecture Notes in Engineering 45, Advances in Fluid Mechanics Measurement*, edited by M. Gad-el-Hak, Springer-Verlag, Berlin Heidelberg, 1989, pp. 33–107.

[4]Jimenez, J., Cogollos, M., Bernal, L. P., "A Perspective View of the Plane Mixing Layer," *Journal of Fluid Mechanics*, Vol. 152, 1985, pp. 125–143.

[5]Agui, J.C., and Hesselink, L., "Flow Visualization and Numerical Analysis of a Coflowing Jet: A Three Dimensional Approach," *Journal of Fluid Mechanics*, Vol. 191, 1988, pp. 19–45.

[6]Drebin, R. A., Carpenter, L., and Hanrahan, P., "Volume Rendering," *Computer Graphics*, Vol. 22, No. 4, Aug. 1988, pp. 65–74.

[7]van Cruyningen, I., Lozano, A., and Hanson, R. K., "Volume Rendering of Multidimensional Fluid Flow Images," *SIGGRAPH Video Reviews #44 - Volume Visualization,* and *SIGGRAPH Video Reviews #42-43 - Visualization in Scientific Computing*, edited by T. S. DeFanti, Association for Computing Machinery: Special Interest Group on Computer Graphics, New York, 1989.

[8]van Cruyningen, I., Lozano, A., and Hanson, R. K., "Computer Rendering of Planar Fluorescence Flowfield Images," AIAA Paper 90-0499, Jan. 1989.

[9]Mungal, M. G., and Hollingsworth, D. K., "Organized Motion in a Very High Reynolds Number Jet," *Physics of Fluids A*, Vol. 1, No. 10, 1989, pp. 1615–1623.

[10]Mungal, M. G., Lozano, A., van Cruyningen, I., "Large-Scale Dynamics in High Reynolds Number Jets and Jet Flames,"*Experiments in Fluids, A* (submitted for publication).

[11]Dimotakis, P. E., Miake-Lye, R. C. and Papantoniou, D. A., "Structure and Dynamics of Round Turbulent Jets," *Physics of Fluids*, Vol. 26, No. 11, Nov. 1983, pp. 3185–3192.

[12]Mungal, M.G., Karasso, P. S., and Lozano, A., "The Visible Structure of Turbulent Jet Diffusion Flames: Large-Scale Organization and Flame Tip Oscillation," *Combustion Science and Technology* (submitted for publication).

[13]Chen, L. D., and Roquemore, W. M., "Visualization of Jet Flames," *Combustion and Flame*, Vol. 66, 1986, pp. 81–86.

[14]Dahm, W. J. A., and Dimotakis, P. E., "Measurements of Entrainment and Mixing in Turbulent Jets," *AIAA Journal*, Vol. 25, Sept. 1987, pp. 1216–1223.

Effect of Fiber Modulus Variations on Stress Concentration in Hybrid Composites

J. N. Rossettos* and K. Sakkas†
Northeastern University, Boston, Massachusetts 02115

Introduction

INTEREST in hybrid composites, where more than one type of fiber material is contained in a common matrix, has been prompted by their ability to provide a balance between stiffness and strength. Also, as indicated in Ref. 1, a hybrid effect can be realized, where the higher-modulus fibers have a larger failure strain than when they exist alone in a nonhybrid composite. Fukuda and Chou[1] use shear lag theory[2] to study the stress concentration near broken fibers in hybrid composite sheets. They introduce the parameter R, which is the ratio of the axial stiffness of the low modulus (*LM*) to high modulus (*HM*) fibers, and gives results for $R = 1/3$, a value typical of carbon/glass hybrids.

The present Note gives results for a full range of values of R, for both two-dimensional (sheet) and three-dimensional configurations. As will be seen, the stress concentration drops for *HM* fibers while it rises for the *LM* fibers as R ranges from 1 to 0.2. Direct solution of a matrix system of differential equations using eigenvector expansions provides a convenient means of analysis. The results reduce to those of Fukuda and Chou[1] for $R = 1/3$ and to those of Hedgepeth[2,3] when $R = 1$.

Analysis

In the lamina analysis, we consider a finite-width sheet consisting of $2q + 1$ fibers parallel to the x axis or load direction. The center fiber is the zeroth, and the fibers above it are numbered so that n equals 1 to q. Below it, they are numbered -1 to $-q$. There is an alternating arrangement of HM and LM fibers, where one or more fibers are broken in a continuous manner at $x = 0$. The axial load and displacement in the nth fiber are denoted by $p_n(x)$ and $u_n(x)$. In what follows, asterisks will also denote quantities related to *LM* fibers. Force equilibrium is based on the well-known shear lag model,[2,3] where fibers take the axial load and the matrix is in pure shear and involves a force balance between the varying fiber load, dp_n/dx, and the shear in the matrix on either side of the fiber. For instance, the shear force per unit length between the nth and $n + 1$th fiber, where the nth fiber is *HM*, is $Gh(u^*_{n+1} - u_n)/d$. It is $Gh(u_n - u^*_{n-1})/d$ between the nth and $n - 1$th fiber; d is the distance between fibers and h is sheet thickness. Equilibrium equations are derived as in Ref. 2 and are given for *HM* and *LM* fibers, respectively, as

$$EA\frac{d^2u_n}{dx^2} + \left(\frac{Gh}{d}\right)(u^*_n - 2u_n + u^*_{n-1}) = 0 \quad (n = 0,2,4, \ldots)$$

$$E^*A^*\frac{d^2u^*_n}{dx^2} + \left(\frac{Gh}{d}\right)(u_{n+1} - 2u^*_n + u^*_{n-1}) = 0 \quad (n = 1,3, \ldots) \tag{1}$$

Received Feb. 5, 1990; revision received Feb. 14, 1990.

*Professor, Department of Mechanical Engineering.
†Graduate Student, Department of Mechanical Engineering.